Pergamon

Geochimica et Cosmochimica Acta, Vol. 62, No. 2, pp. 227–243, 1998

0016-7037/98 $19.00 + .00

PII S0016-7037(97)00336-0

# Chemical weathering in a tropical watershed, Luquillo Mountains, Puerto Rico: II. Rate and mechanism of biotite weathering

Sheila F. Murphy,[1,*,†] Susan L. Brantley,[1] Alex E. Blum,[2,3] Art F. White,[3] and Hailiang Dong[4]

[1]Department of Geosciences, The Pennsylvania State University, University Park, Pennsylvania 16802, USA
[2]U.S. Geological Survey, Boulder, Colorado 80303, USA
[3]U.S. Geological Survey, Menlo Park, California 94301, USA
[4]Department of Geological Sciences, The University of Michigan, Ann Arbor, Michigan 48109, USA

(*Received June* 19, 1996; *accepted in revised form September* 18, 1997)

**Abstract**—Samples of soil, saprolite, bedrock, and porewater from a lower montane wet forest, the Luquillo Experimental Forest (LEF) in Puerto Rico, were studied to investigate the rates and mechanisms of biotite weathering. The soil profile, at the top of a ridge in the Rio Icacos watershed, consists of a 50–100-cm thick layer of unstructured soil above a 600–800 cm thick saprolite developed on quartz diorite. The only minerals present in significant concentration within the soil and saprolite are biotite, quartz, kaolinite, and iron oxides. Biotite is the only primary silicate releasing significant K and Mg to porewaters. Although biotite in samples of the quartz diorite bedrock is extensively chloritized, chlorite is almost entirely absent in the saprolite phyllosilicates. Phyllosilicate grains are present as 200–1000 $\mu$m wide books below about 50 cm depth. X-ray diffraction (XRD) and electron microprobe analyses indicate that the phyllosilicate grains contain a core of biotite surrounded by variable amounts of kaolinite. Lattice fringe images under transmission electron microscope (TEM) show single layers of biotite altering to two layers of kaolinite, suggesting dissolution of biotite and precipitation of kaolinite at discrete boundaries. Some single 14-Å layers are also observed in the biotite under TEM. The degree of kaolinitization of individual phyllosilicate grains as observed by TEM decreases with depth in the saprolite. This TEM work is the first such microstructural evidence of epitaxial growth of kaolinite onto biotite during alteration in low-temperature environments.

The rate of release of Mg in the profile, calculated as a flux through the soil normalized per watershed land area, is approximately 500 mol hectare$^{-1}$ yr$^{-1}$ ($1.6 \times 10^{-9}$ mol$_{Mg}$ m$_{soil}^{-2}$ s$^{-1}$). This rate is similar to the flux estimated from Mg discharge out the Rio Icacos (1000 mol hectare$^{-1}$ yr$^{-1}$, or $3.5 \times 10^{-9}$ mol$_{Mg}$ m$_{soil}^{-2}$ s$^{-1}$), indicating that scaling up from the soil to the watershed is possible for Mg release. The rate of Mg release from biotite, normalized to Brunauer-Emmett-Teller (BET) surface area, is calculated using a mass balance equation which includes the density and volume of phyllosilicate grains, porewater chemistry and flux, and soil porosity. The mean rates of biotite weathering calculated from K and Mg release rates are approximately 6 and $11 \times 10^{-16}$ mol$_{biotite}$ m$_{biotite}^{-2}$ s$^{-1}$ respectively, significantly slower than laboratory rates ($10^{-12}$ to $10^{-11}$ mol$_{biotite}$ m$_{biotite}^{-2}$ s$^{-1}$). The discrepancy in scaling down from the soil to the laboratory is probably explained by (1) differences in weathering mechanism between the two environments, (2) higher solute concentrations in soil porewaters, (3) loss of reactive surface area of biotite in the saprolite due to kaolinite and iron oxide coatings, and/or (4) unaccounted-for heterogeneities in flow path through the soil. *Copyright © 1998 Elsevier Science Ltd*

## 1. INTRODUCTION

The tropical environment is extremely important in understanding global biogeochemical cycles (Meybeck, 1979; Milliman and Meade, 1983), yet little is known about weathering processes and rates at the low latitudes. In order to investigate the rates and mechanisms of chemical weathering in a tropical climate, soil mineralogy and porewater and surface water chemistry from the Rio Icacos watershed in the Luquillo Experimental Forest, a lower montane wet forest in Puerto Rico, were examined. The investigation is part of a larger project associated with the Water, Energy, and Biogeochemical Budgets (WEBB) Program of the U.S. Geological Survey, which assesses the cycling of nutrients and energy within natural systems. The first paper in this series (White et al., 1997) describes chemical mass balances and weathering fluxes in the soils and watershed. The present paper discusses the mechanism and transformations associated with biotite weathering.

Tropical soils are generally depleted in primary minerals and contain large amounts of secondary alteration minerals such as gibbsite, kaolinite, and iron oxides (Kalpage, 1974). Because micas tend to be more resistant to weathering than minerals such as feldspars, hornblende, and pyroxenes (Goldich, 1938), these phyllosilicates are a major reservoir for K in tropical environments and play a significant role in fertility, pedogenesis, and weathering (Rausell-Colom et al., 1965).

### 1.1 Mechanism of Biotite Weathering

The weathering of mica in nonacidic soils most often involves a simple transformation in which the trioctahedral phyllosilicate transforms to expandable 2:1 minerals, such as vermiculite or smectite. Potassium is replaced with hydrated cations, and Fe is oxidized, either by layer or edge weathering

* *Present address:* Shepherd Miller Inc., 3801 Automation Way, Suite 100, Fort Collins, Colorado 80525, USA.
† Author to whom correspondence should be addressed.

(Fanning et al., 1989). Based upon laboratory experiments at pH 4 and above, Acker and Bricker (1992) reported that octahedral cations were preferentially lost from biotite, forming vermiculite as a product. In acidic, highly leached soils, common in the tropics, the 2:1 layer may decompose at the same rate as K is released from the interlayer, or hydroxy-interlayers may form (Fanning et al., 1989). Under such conditions, biotite is thought to be replaced by 1:1 phyllosilicates such as kaolinite or halloysite (e.g., Ojanuga, 1973; Eswaran and Heng, 1976; Ahn and Peacor, 1987). The transformation of biotite to kaolinite is more complicated than that of biotite to vermiculite, for it requires replacement of a 2:1 trioctahedral with a 1:1 dioctahedral phyllosilicate.

Evidence for such a transformation is largely inferential, because the reactants and products are intimately mixed at a scale which cannot be resolved by optical microscopy or electron microprobe (Fordham, 1990). Theories of the alteration include a dissolution/reprecipitation/recombination mechanism, where the biotite structure is reconstituted to kaolinite (Ojanuga, 1973); octahedral cation migration with equilibration by Al ions (Stoch and Sikora, 1976); and epitaxial or topotaxial replacement on preserved anion layers (Gilkes and Suddhiprakarn, 1979). However, controversy exists as to whether, even in those environments where biotite apparently weathers to kaolinite, an intermediate alteration product may form ephemerally.

Rebertus et al. (1986) observed kaolinite retaining the morphology of the biotite precursor but with the optical and structural properties of kaolinite in studies of soils formed from coarse-grained regional metamorphic rocks in the Blue Ridge and Piedmont physiographic provinces of North Carolina, USA. These authors proposed that Al released by biotite weathering precipitates as hydroxy Al in the interlayers of altering biotite, forming a short-lived hydroxy-Al interlayered vermiculite (HIV). This phase then transforms to kaolinite by combining the vermiculite structure with the interlayer hydroxy-Al. The overall reaction, excluding the ephemeral HIV stage, is represented as

$$K_2(Fe_3Mg_3)(Al_2Si_6)O_{20}(OH)_4 + 4Al(OH)_2^+ + 10H^+ \Rightarrow$$
$$1.5Al_4Si_4O_{10}(OH)_8 + 2K^+ + 3Fe^{2+} + 3Mg^{2+} + 5H_2O \quad (1)$$

This reaction requires loss of $K^+$, expansion of biotite structure to that of vermiculite, exchange of interlayer cations and replacement with hydroxy Al, and movement of tetrahedral Al to octahedral positions, resulting in a loss of one of every four tetrahedra (the Al tetrahedron) and inversion of every other silica sheet.

The preceding studies, using electron microprobe, petrographic microscopy, and XRD, only indirectly inferred the transformation of biotite to kaolinite. In hydrothermally altered biotite from the Otago schist, Brighton, New Zealand, Ahn and Peacor (1987) observed with TEM that kaolinite was intimately interstratified with biotite and observed two-layer kaolinite units terminating into single biotite layers. They inferred that one tetrahedral-octahedral-tetrahedral (T-O-T) unit of biotite transformed to two T-O units of kaolinite. This would require replacement of one Fe- and Mg-rich trioctahedral sheet with two aluminous dioctahedral sheets, inversion of one tetrahedral sheet of a T-O-T unit, and replacement of all tetrahedral Al ions with Si. Ahn and Peacor (1987) estimated the reaction involved as

$$K_2(Fe_3Mg_3)(Al_2Si_6)O_{20}(OH)_4 + 6Al^{3+} + 2H_4SiO_4 + 4H_2O \Rightarrow$$
$$2Al_4Si_4O_{10}(OH)_8 + 2K^+ + 3Fe^{2+} + 3Mg^{2+} + 4H^+ \quad (2)$$

This reaction differs from that proposed by Rebertus et al. (1986), Eqn. 1, in that no intermediate HIV step was inferred, and neither Al nor Si is conservative. Ahn and Peacor (1987) proposed that such drastic changes must be caused by dissolution of biotite layers and crystallization of kaolinite layers, and they postulated that a linear discontinuity along reaction boundaries served as the pathway of transport of $H_2O$, Al, and Si entering the structure, and H, K, Fe, and Mg leaving the structure.

The direct biotite-kaolinite transformation inferred in soils may occur based on a reaction similar to that observed for hydrothermal conditions. However, observation of direct biotite/kaolinite transformations under low-temperature conditions has not been previously documented by TEM.

### 1.2. Rate of Biotite Weathering

Several workers have measured or estimated the rate of dissolution of biotite in the laboratory or field (Velbel, 1985; Sverdrup, 1990; Acker and Bricker, 1992; Swoboda-Colberg and Drever, 1993; Turpault and Trotignon, 1994; Kalinowski and Schweda, 1996). Rates are measured in field systems using mass balance methods (see White and Brantley, 1995), or in the laboratory in chemical reactors (Brantley and Chen, 1995) which are run in batch, continuously stirred tank, plug-flow, or fluidized bed mode (Table 1).

Laboratory studies have suggested a weathering product of vermiculite or hydrobiotite (Acker and Bricker, 1992; Kalinowski and Schweda, 1996) or complete dissolution of the structure (Swoboda-Colberg and Drever, 1993). Calculated rates also differ in the component used to determine the biotite dissolution rate. Acker and Bricker (1992), for example, demonstrated that Mg and Fe loss from biotite may occur without substantial dissolution of the tetrahedral sheet and determined rates of release for each component. Because of the ambiguity of defining mica dissolution rate, Kalinowski and Schweda (1996) report rates as weighted mean averages of single element release rates normalized by mineral stoichiometry.

Differences in measured rates also arise because workers report rates normalized by either geometric or BET surface area (Table 1). Surface area has also been measured by chemical adsorption in mineral suspensions (Lowell and Shields, 1991) and radionuclide release and adsorption patterns (Wood et al., 1990). Surface areas estimated by nongeometric methods are higher than geometric areas, probably due to surface roughness related to etch pits (Banfield and Eggleton, 1988) and surface steps (Swoboda-Colberg and Drever, 1993), and also to interlayer surface area (Kalinowski and Schweda, 1996). However, the reactivity of the surface may also vary widely and may be related to the importance of mineral defects (e.g., Brantley et al., 1986), or for minerals such as biotite, the marked structural anisotropies (Turpault and Trotignon, 1994).

Kalinowski and Schweda (1996) support the argument of

Table 1. Weathering rate of biotite measured in laboratory and field experiments.

| Study | pH | Duration of experiment or type of field study | Assumed secondary product | Surface area method | Basis for rate | log rate[3] ($mol_{bio}\ m_{bio}^{-2}\ s^{-1}$) |
|---|---|---|---|---|---|---|
| Laboratory | | | | | | |
| Sverdrup (1990)[1] | 4–4.5 | ? | ? | BET | K and Mg release | −11.4 to −11.0 |
| Acker and Bricker (1992) | 5 | ~5000 h | Hydrobiotite | BET | Mg release | −10.7[4] |
| Swoboda-Colberg and Drever (1993)[2] | 4.5 | ~2000 h | Assumed complete dissolution | Geometric | K release, stoichiometry of biotite assumed | −11.4 |
| Kalinowski and Schweda (1996) | 4.5 | ~1000 h | Decationized residual silicate | BET | Release of all cations | −11.9[5] |
| Field | | | | | | |
| Velbel (1985) | 6 | Watershed | Hydrobiotite | Geometric | Mg release | −13.0 |
| Swoboda-Colberg and Drever (1993)[2] | ~4.5 | Acid application to small plots | Assumed complete dissolution | Geometric | Si flux apportioned among 6 minerals using lab rate ratios | −14.0 |
| This study | ~4.5 | Solute flux through soil profile | Kaolinite | BET, Normalized for biotite/ kaolinite ratio | Mg release rate | −15.0 |

[1] As cited in Swoboda-Colberg and Drever (1993).
[2] Study used the same minerals for laboratory and field measurements.
[3] Assuming a formula unit of $O_{10}(OH)_2$.
[4] Assumed stoichiometric dissolution as per authors' conclusion statements, and assumed $O_{10}(OH)_2$ as the mineral stoichiometry.
[5] Reported by the authors as a weighted average of element release rate normalized by stoichiometry of biotite, and normalized by initial surface area.

Turpault and Trotignon (1994) that biotite weathering is dominated by reactions at edge sites. Rates are, therefore, dependent upon edge site density and are not linearly dependent upon total surface area. These authors also reported a factor of 2 increase in surface area during dissolution, which was attributed partly to delamination along basal structures. Despite the many ambiguities in biotite weathering studies in the laboratory, the resulting release rates (normalized by geometric or BET surface area) are on the order of $10^{-12}$ to $10^{-11}$ $mol_{biotite}\ m_{biotite}^{-2}\ s^{-1}$ at pH 4–5 (Table 1).

Natural weathering rates of most silicates, including biotite, estimated from mass balance calculations using surface and groundwater ion concentrations, are smaller than those of laboratory dissolution studies by several orders of magnitude (Table 1; see also White and Brantley, 1995). This discrepancy may be explained by differences in reaction mechanism, errors in estimation of appropriate field parameters, differences in solution chemistry (including background electrolytes, organic acids, and chemical affinity), discrepancies in surface area estimation, inhomogeneities in estimated flow paths, temperature differences, or biological factors (Brantley, 1992; van Grinsven and van Riemsdijk, 1992; Anbeek, 1993; Swoboda-Colberg and Drever, 1993; White, 1995).

For example, the presence of higher K concentrations in some soil solutions (as compared to laboratory solutions) may reduce the rate of weathering of micas (Rausell-Colom et al., 1965) as compared to dissolution in the laboratory. Due to the slow reaction rate of mica, laboratory investigations of mica dissolution (Table 1) are often carried out at above-ambient temperatures or pressures, or low pH. Lin and Clemency (1981) argued that the extrapolation of these rates to natural weathering conditions may be invalid, as may be the use of pH buffers. Acker and Bricker (1992) found that biotite dissolution rates increased and the mechanism of dissolution changed as pH decreased from 7 to 3. Studies of the effect of organic acids on mica dissolution revealed that high concentrations of fulvic, humic, and acetic acids increased the rate of dissolution (Schnitzer and Kodama, 1976; Tan, 1980). Plant and biological conditions also affect the rate of biotite breakdown (e.g., Rausell-Colom et al., 1965; Sawhney and Voigt, 1969).

In this paper, we investigate the rate and mechanism of biotite weathering in a tropical soil and compare the rate estimated in the soil and saprolite to the mineral surface area-normalized rate predicted in laboratory experiments, as well as to the land surface area-normalized rate observed at the watershed scale. Prediction of mineral weathering rates at different scales of observation are of importance in answering questions bridging regional, continental, and global geochemical cycling.

## 2. Geologic Setting

The Luquillo Mountains are characterized by rugged topography and elevations reaching 1,074 m above sea level (Fig. 1a). Soil and porewater samples described in this paper were collected from the LG-1 sampling site, described in greater detail by White et al. (1998). The site is located on a ridge between two first-order tributaries on the eastern side of the Rio Icacos basin (Fig. 1b). The Rio Icacos watershed is entirely underlain by quartz diorite of the Tertiary Rio Blanco stock. Overlying soils are ultisols and are part of the Utuado series, belonging to the Utuado-Picacho-Stony rock land association (Boccheciamp, 1977). The unstructured, bioturbated soil is

50–100 cm thick. Below this depth exists a 600–800 cm-thick zone of saprolite. Saprolite is defined as a clay-rich, thoroughly decomposed rock that still retains evidence of bedrock structure and is presumed to be formed in place by chemical weathering of the bedrock (American Geological Institute, 1976). The depth to bedrock varies from 300 to 1000 cm in the surrounding ridge-top area. In this paper, the combined soil and saprolite horizons will be referred to as regolith.

Mineralogy and chemistry of the profile is described in detail by Murphy (1995) and White et al. (1998). The bedrock consists of quartz, plagioclase, hornblende, and biotite, with minor K-feldspar and accessory phases. Saprolite mineralogy consists of primary quartz and altered biotite, as well as fine-grained kaolinite and iron oxyhydroxides. Very limited amounts (<1%) of plagioclase and K-feldspar were identified in the saprolite by X-ray diffraction (XRD) and saprolite microprobe mounts (White et al., 1998). Altered biotite grains were easily distinguishable by eye as bronze-colored books (referred to below as phyllosilicate grains) and were observed at all depths below approximately 50 cm in the profile. Between the bedrock and saprolite is a zone tens of centimeters thick saprock, which is cohesive, lighter in color, and in which nearly all of the feldspars are weathered to kaolinite. Unfortunately, it was not possible to quantitatively sample this zone at the time of field work.

## 3. ANALYTICAL METHODS

Sampling of bedrock from directly below the regolith profile was not possible due to the excessive regolith thickness and rugged, remote site location. Fresh bedrock samples were obtained from a roadcut very near the profile site (Fig. 1b). Chemical composition of biotite in bedrock was determined by Cameca SX-50 electron microprobe in polished section. Biotite grains were also hand-picked from crushed bedrock, ground in acetone, and analyzed by X-ray diffraction (XRD) in oriented samples on a Rigaku X-ray using a Cu filament and Ni filter. Narrow slits were used to enhance low angle resolution.

In the regolith, macroscopic phyllosilicate grains (>~100 $\mu$m diameter) were separated as described by White et al. (1998). Iron oxides were removed with citrate-bicarbonate-dithionite (CBD) treatment (Mehra and Jackson, 1960). The densities and surface areas of phyllosilicate grains were estimated by pycnometer (Hutchison, 1974) and by the BET method (using $N_2$), respectively. Grains used for ferrous/ferric iron determination analysis were hand-picked from the regolith and were not dithionite-treated so that oxidation state was retained. These grains were ground to <100 mesh in an $N_2$-glove box to prevent iron oxidation.

Chemical compositions of the regolith phyllosilicate grains were determined with X-ray fluorescence (XRF) by XRAL Laboratories (Golden, CO). FeO content of the phyllosilicate grains was determined by the Goldich (1984) method of dichromate titration, total Fe by $LiBO_2$ fusion, and $Fe_2O_3$ by difference. CBD-cleaned phyllosilicate grains were ground and analyzed in parallel orientation with XRD in the same manner as bedrock biotite grains. Phyllosilicate grains were also analyzed by XRD after $Mg^{2+}$ saturation, $Mg^{2+}$ saturation/ethylene glycol solvation, $K^+$ saturation, and $K^+$ saturation/heating to 110°C and 550°C, according to methods detailed by Whittig and Allardice (1986). Morphology and qualitative chemical composition of carbon-coated phyllosilicate grains were determined on an International Scientific Instruments (ISI) SX 40A Scanning Electron Microscope with an Energy Dispersive X-ray attachment (SEM-EDX) and with electron microprobe.

Transmission electron microscope (TEM) analysis of samples from depths of 135 cm, 452 cm, and 714 cm was performed at the Electron Microbeam Analysis Laboratory (EMAL) at the University of Michigan. Thin-sections were made with the surface approximately perpendicular to the (001) face of resin-imbedded phyllosilicate grains. Phyllosilicate grains were then optically examined, removed from thin section, ion-milled, and carbon-coated. TEM observations were made with a CM12 scanning-transmission electron microscope (STEM) fitted with a solid-state detector for X-ray energy dispersive analysis. The STEM was operated at a voltage of 120 kV and a current of 20 $\mu$A. Most of the TEM images were obtained at $10^5\times$ magnification. A camera length of 770 mm and a selected area aperture of 10 $\mu$m were used to obtain selected area electron diffraction (SAED) patterns. Quantitative chemical analyses were made in STEM-EDS mode with a beam diameter of 50 Å and a scanning area of 200 × 200 Å. Standards and procedures for interpretation of spectra are defined in Jiang et al. (1990). It was difficult to image kaolinite layers due to rapid electron-beam damage. Pure kaolinite packets were destroyed by the electron beam more rapidly than the kaolinite layers interleaved with the biotite layers.

## 4. RESULTS

### 4.1. Bedrock Biotite Mineralogy

Optical microscopy showed bedrock biotite to be light to medium brown, with green alteration. Back-scattered electron (BSE) images of the bedrock reveal interlayered dark and light phases in a single biotite grain (Fig. 2a). The phases are large enough to determine chemical compositions of the separate phases with an electron microprobe (Table 2). The light area (high in Ti, K) has a biotite-like composition, while the dark area (low in Ti, K, and high in Fe, Mg) is inconsistent with biotite composition. STEM analyses of 10.0-Å layers of biotite gave a composition similar to that determined by electron microprobe and revealed that the Ti is part of the biotite structure and is not due to solid inclusions (Dong et al., 1998). XRD analyses of hand-picked biotite grains from crushed bedrock revealed peaks at both 10.0 and 14 Å (Fig. 2b). The 10.0-Å peak is due to biotite; this peak lies between the (001) peak of Fe-rich mica, annite, and that of the Mg-rich mica, phlogopite.

The 14-Å peak, which is much less intense than the 10.0-Å peak, could indicate chlorite or vermiculite. XRD analysis of Mg-saturated bedrock biotite grains was inconclusive, due to the difficulty of obtaining enough biotite from hand-picking and retaining this material throughout cation treatment. However, the intensity of the (002) peak in the pattern shown in Fig. 2b is much greater than that of the (001) peak, suggestive of chlorite. Also, the mole ratio of (Mg + Fe + Al + Ca)/Si for the dark region observed with microprobe is 2.2 in comparison to the ranges of 1.9–4 for chlorite, and 1.5–1.7 for vermiculite (Deer et al., 1992). Furthermore, igneous biotite commonly undergoes postmagmatic autometamorphism to chlorite during cooling (Speer, 1984). It is, therefore, concluded that the dark regions in the BSE images are chlorite.

### 4.2. Saprolite Phyllosilicate Mineralogy and Chemistry

#### *4.2.1. Physical and chemical analysis*

In the regolith, the most visible mineral grains are phyllosilicate books 200–1200 $\mu$m in diameter located from 50 cm depth to the saprolite/bedrock interface (Fig. 3). The phyllosilicate grains are mostly golden-colored, often with reddish-brown coatings of iron oxide on the edges, suggesting that some iron ejected from the structure may have been precipitated locally. Due to heterogeneity of grains, exact density or density variation with depth could not be determined; however,

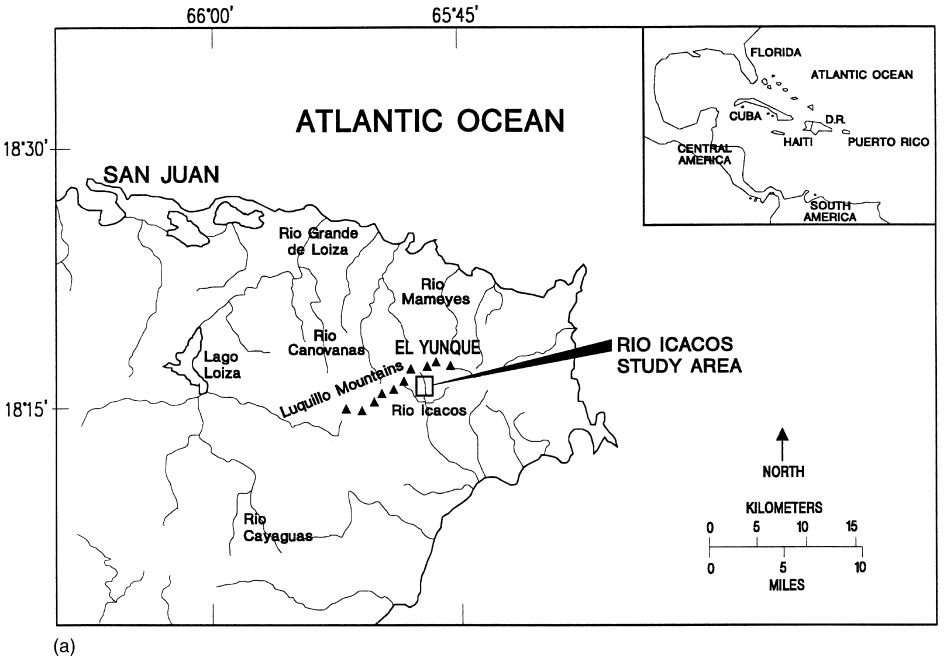


(a)

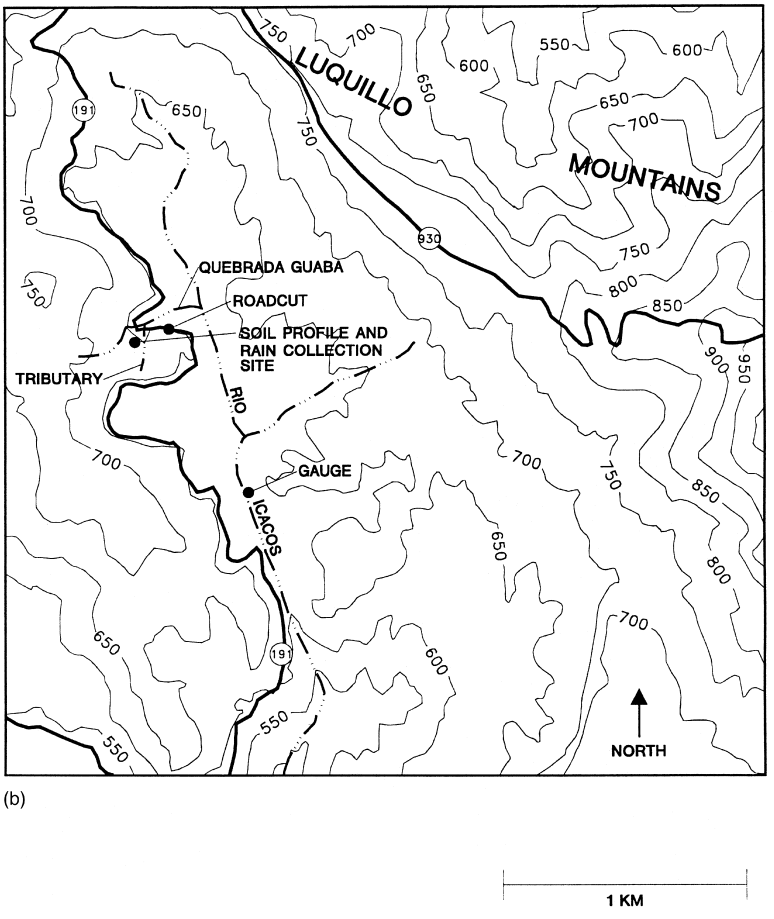


(b)

Fig. 1. (a) Location map of study site. The Luquillo Mountains are located on the eastern edge of Puerto Rico in the Luquillo Experimental Forest, known colloquially as El Yunque. The site is located in the El Yunque quadrangle (18° 15′N, 65° 50′ W). (b) Regolith samples were taken from a slope of 30° at an elevation of 670 m. Fresh bedrock samples were taken from a roadcut near the regolith profile. Stream water samples were collected from the Quebrada Guaba, 40 m downslope from the regolith profile site.

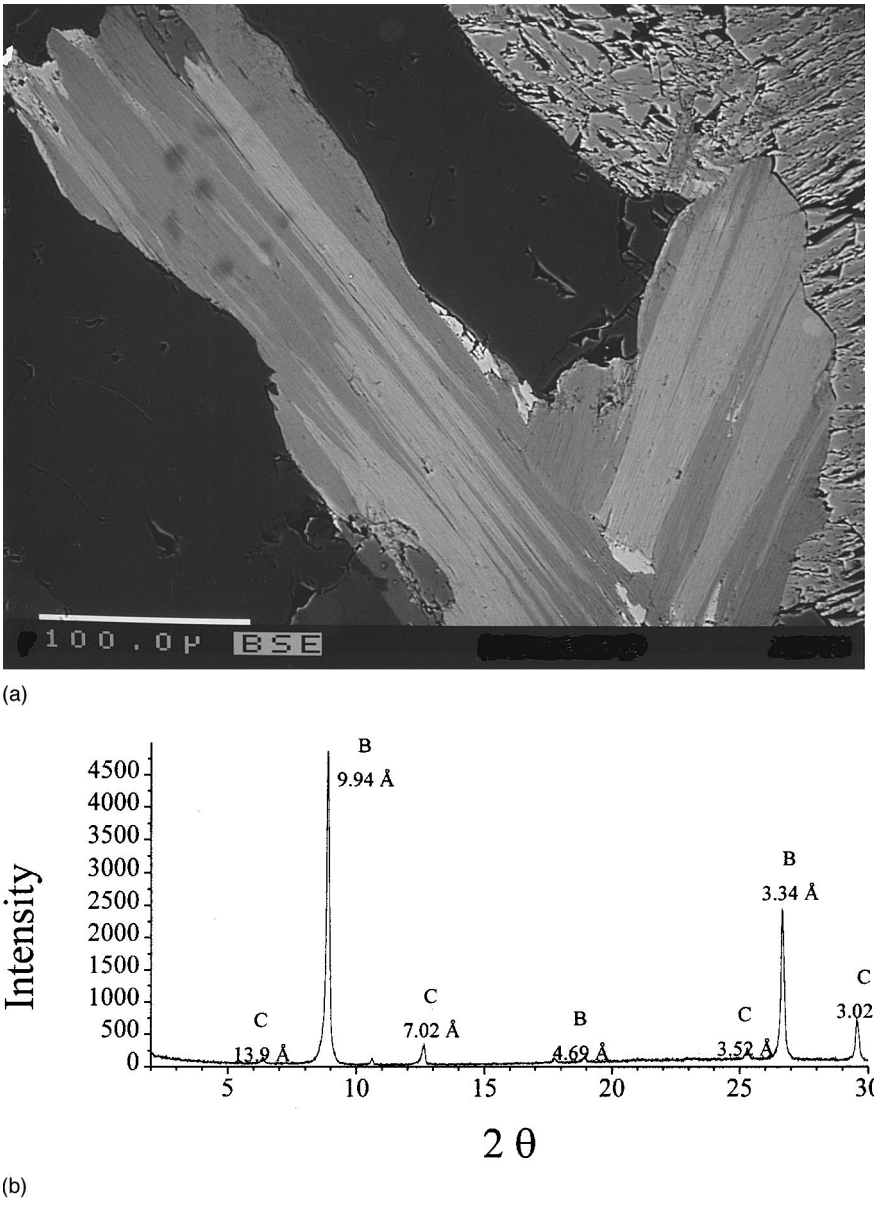


Fig. 2. (a) Back-scattered electron microprobe image of the bedrock biotite. Bright and dark regions have typical biotite and chlorite-like compositions, respectively. Note random, patchy nature of the chlorite alteration in the grain. (b) XRD pattern of bedrock biotite grains. B and C indicate biotite and chlorite peaks, respectively.

average density was ~2.5 g $cm^{-3}$. Surface areas of phyllosilicate grains from depths of 137 and 714 cm were 8.3 and 8.1 $m^2$ $g^{-1}$ respectively, as measured by BET.

With increasing distance above the bedrock/saprolite interface, the relative weight percent (as measured by XRF) of $K_2O$, $TiO_2$, and MgO in phyllosilicate grains decrease, and weight percent of $Al_2O_3$ increases (Murphy, 1995). A significant decrease in octahedral cation concentration occurs above a depth of 450 cm, which correlates with the zone of lowest water content in the profile and low porosity (White et al., 1998). However, the number of moles of Mg, K, Si, and Al relative to Ti in phyllosilicate grains are fairly constant as a function of depth (Fig. 4a and 4b). White et al. (1998) show convincing evidence that Ti is conservative in the bulk soil within the saprolite zone.

The surface area given above is not likely due entirely to biotite, but to kaolinite within and coating the biotite and also to cracks and pores in the grain (discussed below). Therefore, the proportion of biotite in the phyllosilicate grains at depth, $X_{bio}(z)$, was estimated. Based on the low Ti content of the kaolinite (Table 2), all Ti in the phyllosilicate grains (measured by XRF) was assumed to be in the biotite. The amount of Si required to fill the saprolite biotite formula (Table 2), based on the measured Ti, was subtracted from the total Si content in the grains. The remaining Si was assumed to be in kaolinite. The moles of biotite and kaolinite were calculated from the amount

Table 2. Microprobe and STEM chemical analyses of saprolite and bedrock phyllosilicate grains

| | Oxide weight percent | | | | |
|---|---|---|---|---|---|
| Element | Bedrock biotite[1] | Bedrock chlorite[1] | Saprolite biotite[2] | Saprolite kaolinite (720 cm)[2] | Saprolite kaolinite (450 cm)[2] |
| Si | 37 | 29 | 46 | 51 | 56 |
| Ti | 4 | 0.2 | 3 | 0.7 | 0.0 |
| Al | 15 | 19 | 24 | 37 | 36 |
| Mg | 11 | 14 | 5 | 1.2 | 0.7 |
| Fe | 22 | 26 | 9 | 4.2 | 2.1 |
| K | 9 | 0.1 | 7 | 0.9 | 0.1 |

Derived formulas:
Bedrock biotite: $K_{0.85}(Al_{0.10}Ti_{0.20}Fe^{2+}_{1.30}Fe^{3+}_{0.05}Mg_{1.25})(Si_{2.8}Al_{1.2})O_{10}(OH)_2$
Saprolite biotite: $K_{0.65}(Al_{1.10}Ti_{0.15}Fe^{2+}_{0.35}Fe^{3+}_{0.15}Mg_{0.55})(Si_{3.2}Al_{0.8})O_{10}(OH)_2$
Saprolite kaolinite[3] (720 cm): $(K_{0.04}Fe_{0.14}Ti_{0.02}Mg_{0.07})(Si_{2.02}Al_{1.72})O_5(OH)_4$
Saprolite kaolinite[3] (450 cm): $(K_{0.01}Fe_{0.07}Mg_{0.04})(Si_{2.21}Al_{1.69})O_5(OH)_4$

Formula for bedrock chlorite not determined as structural division of Mg is unknown.
[1] Analyzed by electron microprobe.
[2] Analyzed by STEM.
[3] Cation concentrations and high Si/Al ratio suggest contamination of this measurement with other phases.

of Si in their formulas, converted to volumes, and the ratio of biotite to biotite + kaolinite was calculated.

This estimate reveals that the fraction of biotite in the grains varies from <15% to approximately 30% of the total volume (Fig. 4c). The calculation indicates that the higher the modal abundance of phyllosilicate grains in the regolith, the lower the proportion of biotite in the grains (Murphy, 1995). Above a depth of 120 cm, the proportion of biotite in the phyllosilicate grains increases towards the surface of the profile (Fig. 4c), perhaps due to comminution of kaolinite in the bioturbated zone.

Wet chemistry showed $Fe^{2+}$ to comprise approximately 6.6% of the total Fe in the phyllosilicate grains, with no variation observed with depth (Murphy, 1995). However, because the phyllosilicate grains used for Fe determination were not dithionite-treated, much of the $Fe^{3+}$ may be present as iron oxide coatings or as inclusions of magnetite (see, in contrast, the ferrous/ferric ratios calculated from TEM data, Table 2). Also, SEM-EDX analysis of phyllosilicate grains revealed Fe-rich inclusions, which are probably oxides formed from iron released from the weathering of biotite.

### *4.2.2. SEM and electron microprobe analysis*

Phyllosilicate grains in the regolith are often thin in the center and widen out to edges approximately twice as thick (Fig. 3a). Layers of the phyllosilicate grains appear continuous from the thin interior to the thicker edges. SEM-EDX analyses revealed that the centers of many grains have biotite-like compositions, whereas the wider edges are kaolinite-like. Element mapping of the basal plane of a grain taken from just above the bedrock/saprolite interface revealed a zone of high K and Mg content and low Al content (indicative of biotite), that is surrounded by a zone of low K and Mg content, high Al content (indicative of kaolinite) (Murphy, 1995).

### *4.2.3. X-ray diffraction analysis*

XRD analysis of the separated phyllosilicate grains from all depths between 53 cm and 720 cm (Fig. 5a) reveals reflections

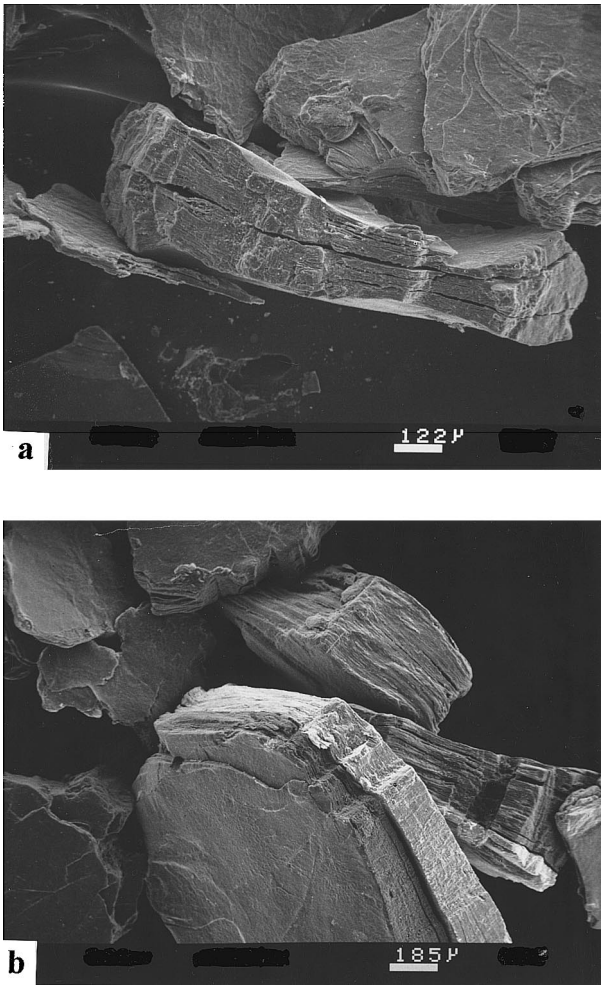


Fig. 3. SEM image of phyllosilicate grains from regolith. Such grains are present from a depth of 56 cm to the bottom of the saprolite. (a) Grain from 714 cm depth. Thin center consists mainly of altered biotite, while thicker edges consist mainly of kaolinite. (b) Grain from 66 cm depth.

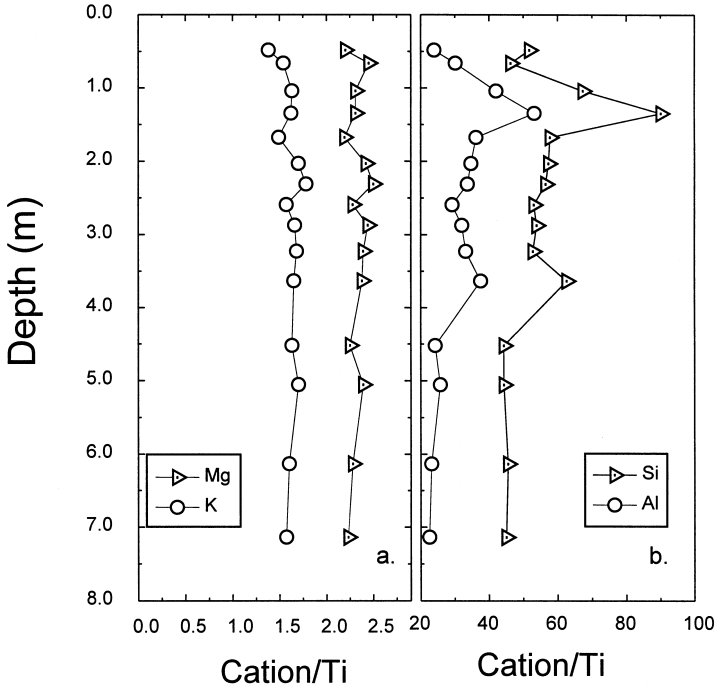


Fig. 4. Calculated ratio of (a) Mg/Ti, K/Ti and (b) Si/Ti, Al/Ti vs. depth in phyllosilicate grains in regolith; (c) calculated volume fraction of biotite/total phyllosilicate as a function of depth in regolith.

at 10.5 Å and ~7.2 Å (varying from 7.1 to 7.4 Å), indicating the presence of both a biotite-like mineral and kaolinite. XRD patterns of single grains also revealed both the 10.5- and ~7.2-Å peaks, indicating that both altered biotite and a kaolinite-family mineral coexist within individual grains. No 14-Å peak was observed, suggesting that there is little or no discrete vermiculite or chlorite in the weathered phyllosilicate grains. The (060) peak of the phyllosilicate grains appears at 1.55 Å and does not shift with depth, indicating a trioctahedral structure with no transformation to a dioctahedral structure with progressive weathering.

Early weathering of biotite usually involves the oxidation of $Fe^{2+}$ to $Fe^{3+}$, which reduces the layer charge, and commonly forms a biotite/vermiculite mixed-layer phase (e.g., Moore and Reynolds, 1989). There was no 24-Å peak observed when the grains were saturated with Mg (Fig. 5b), indicating no evidence for the presence of hydrobiotite (a regular interstratification of mica and vermiculite with the 10-Å spacing of biotite + 14-Å spacing of vermiculite; Sawhney, 1989). Furthermore, the 10.5-Å (001) peak did not shift upon $Mg^{2+}$ saturation, $Mg^{2+}$ saturation/ethylene glycol solvation, $K^+$ saturation, or $K^+$ saturation and heating to 110°C (Fig. 5b). This suggests the absence of regularly or randomly interstratified vermiculite based upon the most common XRD diagnostic techniques for the detection of vermiculite (e.g., Malla and Douglas, 1987).

However, some XRD results do suggest the presence of a randomly interstratified phase with a spacing of ~14 Å: the broad peak at 10.5 Å, and the peak at 3.37 Å, which is narrower and not a multiple of the 10.5-Å peak. These results are consistent with Mérings principles (summarized by Moore and Reynolds, 1989), which state that reflections of randomly interstratified phases will occur between the $(00\ell)$ reflections of the endmember phases, with the positions shifted approximately in proportion to the abundance of the endmembers, and that the broadness of the reflection is a function of the difference in $2\theta$ between the $(00\ell)$ reflections. Thus, the (001) spacing of a 10.0-Å biotite mixed with a small proportion of interstratified 14-Å vermiculite should produce a broad reflection shifted to a position slightly >10.0 Å; the peak position at 10.5 Å suggests about ~12% vermiculite. Likewise, the (003) spacing of 10.0-Å biotite at 3.33 Å and (004) spacing of 14-Å vermiculite at 3.50 Å should produce a relatively narrow reflection shifted to a spacing slightly >3.33 Å, which is consistent with the observed XRD reflection at 3.37 Å.

Upon $K^+$ saturation and heating to 550°C, the 10.5-Å peak collapses to 10.0 Å, and becomes much narrower, symmetric, and increases in intensity, looking like an unaltered biotite peak. This observation is consistent with the presence of some randomly interstratified vermiculite in which an Fe/Al hydroxide has replaced the interlayer cations with a structure which resembles chlorite (Douglas, 1989; Moore and Reynolds, 1989). The hydroxide layer, if present, should not be susceptible to adsorption and exchange reactions and would be stable at 110°C, but would decompose at <550°C to yield a 10-Å structure. The XRD patterns were investigated in more detail using synthetic XRD patterns calculated using NEWMOD© (Reynolds, 1985). Biotite with a 10-Å basal spacing randomly interstratified with ~15% 14-Å layers was required to match the 3.37-Å reflection. However, if the hydroxy-interlayer greatly exceeded 50%, the 10.5-Å reflection shifted to smaller spacings, while the 3.37-Å peak remained nearly unchanged. Thus, the most consistent fit between the synthetic and observed peak shapes and positions suggests that ~15% of the layers are 14-Å hydroxy-interlayer vermiculite with a chlorite-

like structure in which the hydroxides occupy ~50% of the interlayer (as opposed to ~100% in chlorites), forming a pillared-type structure.

#### *4.2.4. TEM analysis*

TEM observations of phyllosilicate grains from depths of 137, 452, and 720 cm in the saprolite indicate that many of the mica grains consist of complex interlayers of 10.5-Å (altered biotite) and 7-Å layers (kaolinite). Some of the grains are composed entirely of altered biotite, with no kaolinite alteration, whereas others are completely altered to kaolinite. Packets of 10.5-Å and 7-Å layers are observed in all three samples, but the proportion of 10.5-Å spacings in the grains increases with depth of saprolite. Some grains also contained single, randomly interstratified 14-Å layers with an abundance of around 7%. The TEM measurement of 10.5-Å spacings in the altered biotite (also see Dong et al., 1998) is not compatible with the XRD patterns. A 10.5-Å biotite should have a (003) spacing of 3.5 Å; a 14-Å vermiculite would have a (004) spacing of 3.5 Å also. Thus, a random interstratification of these phases should produce a narrow and intense XRD reflection at 3.5 Å, whereas the reflection is observed at 3.37 Å. Therefore, the XRD data strongly suggests the absence of an abundant 10.5-Å phase, while TEM measurements consistently show a 10.5-Å phase. While there are differences between the XRD and TEM measurements which could possibly induce structural changes, particularly the effects of the TEM vacuum and the interaction of the electron beam with the sample (especially with Fe), we have not been able to satisfactorily reconcile the contradiction between the TEM and XRD observations with a specific proposed structure.

A variation in composition and layer spacing from edge to center of phyllosilicate grains was observed with TEM. Figure 6a shows a TEM image of a phyllosilicate grain from a depth of 720 cm. The right region of the grain (marked Kaol) contains mainly 7-Å layers (Fig. 6b); STEM-EDS analyses reveal a kaolinite-like composition (Table 2). Further into the grain (Bio + Kaol, Fig. 6c), both 10.5- and 7-Å layers are present, and STEM-EDS analyses revealed a composition midway between the compositions of kaolinite and biotite. In the left region of the grain (Bio), only 10.5-Å layers are visible, and STEM-EDS analyses reveal a biotite-like composition (Fig. 6d). Single 14-Å layers are also visible, occurring about one every thirteen 10.5-Å layers. The width of an altered biotite packet increases toward the left (center of the grain), whereas the kaolinite packet directly next to it follows the opposite trend, widening to the right (Fig. 6c). At the altered biotite/kaolinite interface, single 10.5-Å layers were observed to terminate between two layers of approximately 8.5 Å (Fig. 6c, see arrow), which thin to a thickness of 7 Å to the right.

The composition of the altered biotite is much different than that of the bedrock biotite (Table 2). The altered biotite contains a lower amount of K, and the composition suggests vacancies in the octahedral sites, in contrast to the trioctahedral nature suggested by XRD. The oxidation of Fe is likely to have reduced the fixed charge and decreased the amount of interlayer K. The altered biotite is also highly enriched in Al relative to Si and all the other elements. This may reflect the presence of Al-hydroxy interlayers in a 14-Å phase, as suggested by both the TEM and XRD data, but could also result from the inclusion of a small amount of kaolinite in the STEM measurements. Either source of additional Al may explain the apparent vacancies in the octahedral sites when the bulk composition is converted to a biotite stoichiometry. The presence of Al-hydroxy interlayers may also explain some of the low K occupancy in the exchange sites. While Mg/Si and Fe/Si ratios of altered biotite is different than that of the bedrock biotite, the Ti:Si ratios of bedrock and saprolite biotite remain similar (Table 2).

Observation of the edges of grains from a depth of 137 cm (not shown) revealed coarse kaolinite that was not in the same crystallographic orientation as the biotite. It is possible that this kaolinite precipitated from solution onto the grains. Also, in some grains, lenses of phyllosilicate minerals were observed between areas of kaolinite (Fig. 6b, see arrows). The spacing of layers within the lenses is approximately 7 Å; however, the lenses are not wide enough to determine chemical composition. These lenses are very thin in the deepest sample and are wider and more prevalent in the shallow sample. TEM observations of the phyllosilicate grains are further discussed in Dong et al. (1998).

### 4.3. Porewater Chemistry

Temporal and spatial chemical distributions in porewater at the LG-1 site are discussed in detail by White et al. (1997) in this volume. Porewater pH is moderately acidic (4.5–6.3) and generally increases with depth. Solute concentrations of all other inorganic ions are higher and exhibit greater variability at regolith depths above 120 cm than below this depth. The shallow zone corresponds to the rooting depths of most vegetation (Brown et al., 1983) and is most influenced by evapotranspiration and biogeochemical cycling. Below 120 cm, the concentrations of Si, Mg, and K in porewaters increase with depth. The concentrations of Mg and K in deeper saprolite porewaters are greater than the corresponding Mg and K concentrations in the Rio Guaba and tributary stream adjacent the Guaba Ridge (White et al., 1998, cf. Table 5). In contrast, concentrations of Si, Ca, and Na are lower in the porewaters relative to the stream waters. Mass balance calculations presented by White et al. (1998) indicate that the porewater chemistry is dominated by the dissolution of biotite and quartz in the saprolite and that the stream water chemistry is dominated by dissolution of plagioclase in the quartz diorite bedrock. Linear regression fits to concentration vs. depth data for all samples below 120 cm yield slopes of 28, 8, and 5 $\mu$M/m Si, Mg, and K. At 120 cm, Si, Mg, and K concentrations are 60.7, 18.9, and 5.2 $\mu$M (White et al., 1998, cf. Tables 4 and 5). Solubility calculations indicate the porewaters are supersaturated which respect to kaolinite (White et al., 1998).

## 5. DISCUSSION

### 5.1. Mechanism of Biotite Transformation

The near-complete absence of any discrete chlorite in the saprolite phyllosilicates greatly contrasts with the abundance of this phase observed in one sample of the unaltered bedrock. Therefore, rapid dissolution and/or alteration of chlorite must occur in the transitional bedrock/saprolite zone (tens of cms

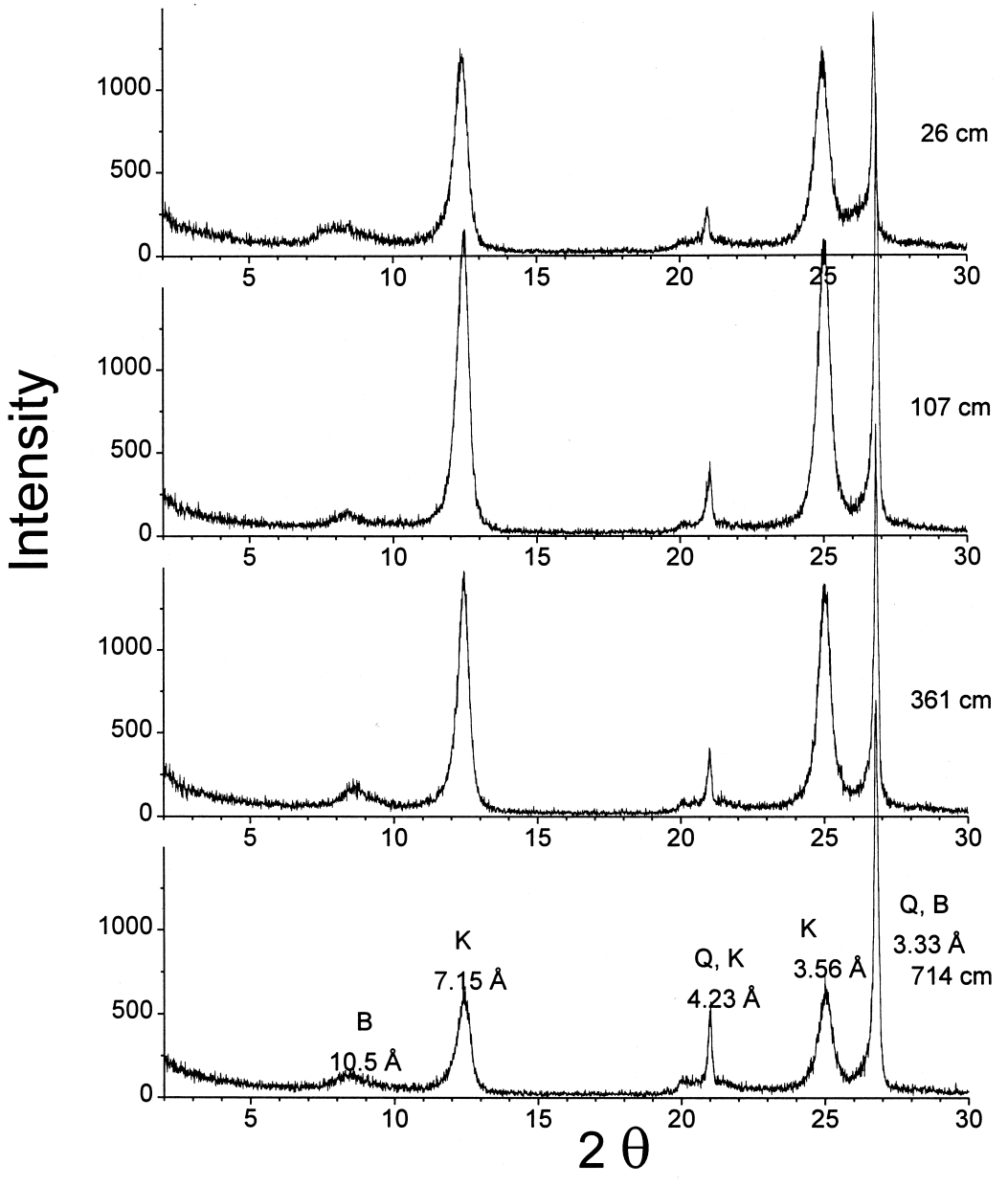


(a)

Fig. 5. (a) XRD patterns of phyllosilicate grains from varying depths in the regolith profile. Grains were CBD-treated and ground under acetone. B indicates biotite peaks, located at 10.5 and 3.33 Å; K indicates kaolinite peaks, located at 7.15, 4.23, and 3.56 Å; Q indicates quartz peaks, which distort the kaolinite and biotite peaks at 4.23 and 3.33 Å. It is likely that a small amount of quartz is included within the phyllosilicate grains. (b) XRD patterns of saturation and glycolation of phyllosilicate grains. B indicates biotite peak; K indicates kaolinite peak. The 10.5-Å biotite (001) peak did not shift upon $Mg^{2+}$ saturation, $Mg^{2+}$ saturation/ethylene glycol solvation, $K^{+}$ saturation, or $K^{+}$ saturation and heating to 110°C. Upon $K^{+}$ saturation and heating to 550°C, the kaolinite peaks are greatly diminished, and the 10.5-Å peak of biotite collapsed to 10.0 Å, became much more symmetric, and increased in intensity.

thick at site LG-1), which were unobtainable for the present study. In this zone, chlorite appears to have completely altered to kaolinite, perhaps explaining some of the intermingling of biotite and kaolinite regions within the phyllosilicate grains. The rapid weathering of chlorite relative to biotite is consistent with other evidence. Experimental data suggests that Mg-rich chlorites have dissolution rates comparable to biotites (May et al., 1995), but that Fe-rich chlorites such as present in this bedrock (Table 2), dissolve 2–3 orders of magnitude faster than biotites (Nagy, 1995). Mafic chlorites have also been observed to be highly unstable in soils (Borchardt, 1989).

SEM and TEM analyses suggest that biotite is weathering directly to kaolinite in the saprolite. The composition of the phyllosilicate grains in the saprolite varied from a kaolinite-like

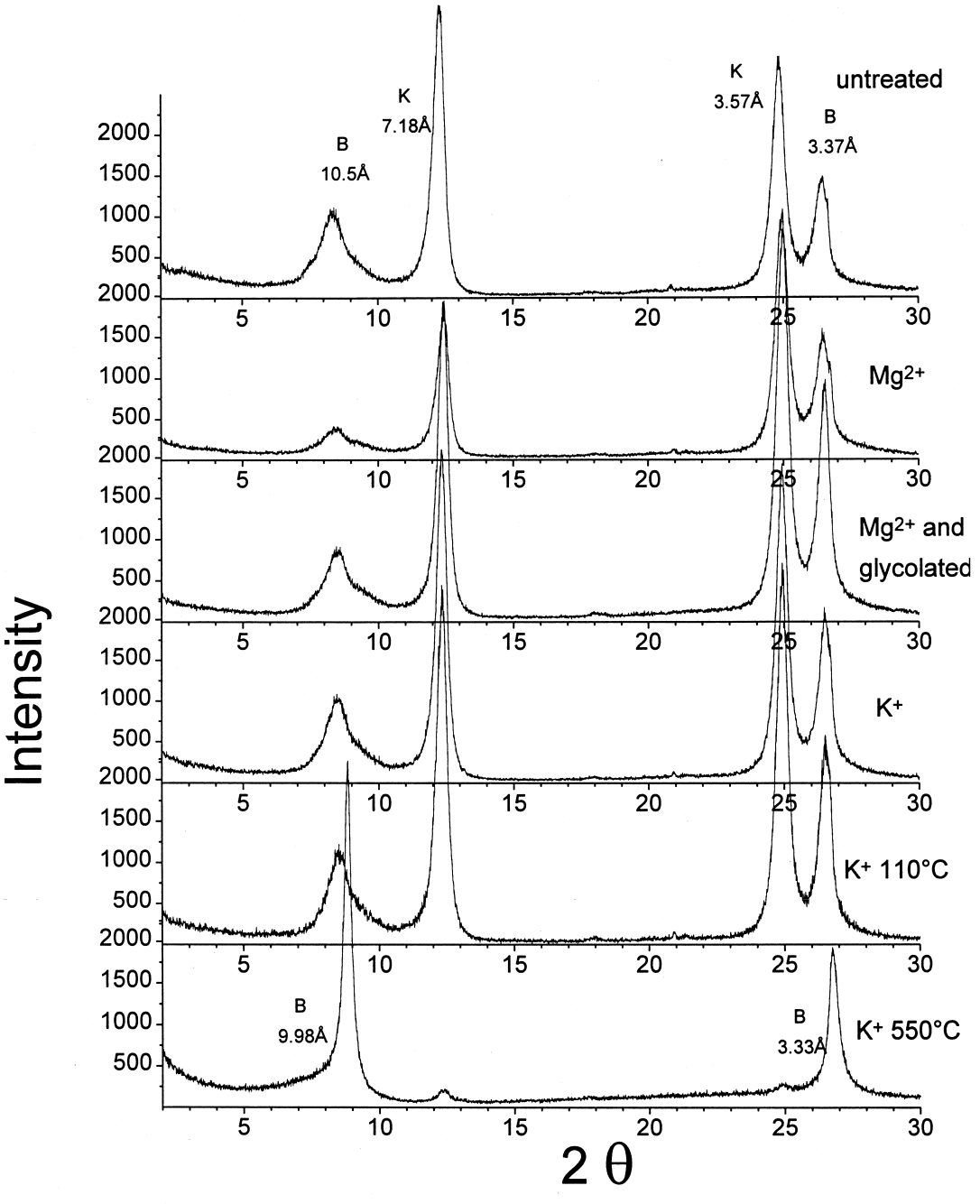


(b)

Fig. 5. (Continued)

composition at the edges to a biotite-like composition at the center (Figs. 3, 6), whereas the composition of the phyllosilicate grains in the bedrock samples was patchy in distribution, without a variation from center to edge (Fig. 2a). Furthermore, we observed under TEM that the extent of kaolinitization of phyllosilicate grains increased from the deeper to the shallower depths in the saprolite, consistent with biotite altering directly to kaolinite in the saprolite zone. The presence of the 14-Å layers in the phyllosilicates may be vermiculite, an intermediate phase in the weathering of biotite to kaolinite; however, TEM images show the direct weathering of biotite layers to kaolinite layers.

The observed transformation of one biotite to two kaolinite layers is similar to that seen by Ahn and Peacor (1987) in a hydrothermally altered biotite. Those workers suggested that due to the drastic chemical and layer thickness changes required in the transformation, the reaction must involve biotite dissolution and kaolinite precipitation. However, whereas Ahn and Peacor (1987) observed one 10-Å layer transforming directly into two 7-Å layers, we observed intermediate 8.5-Å

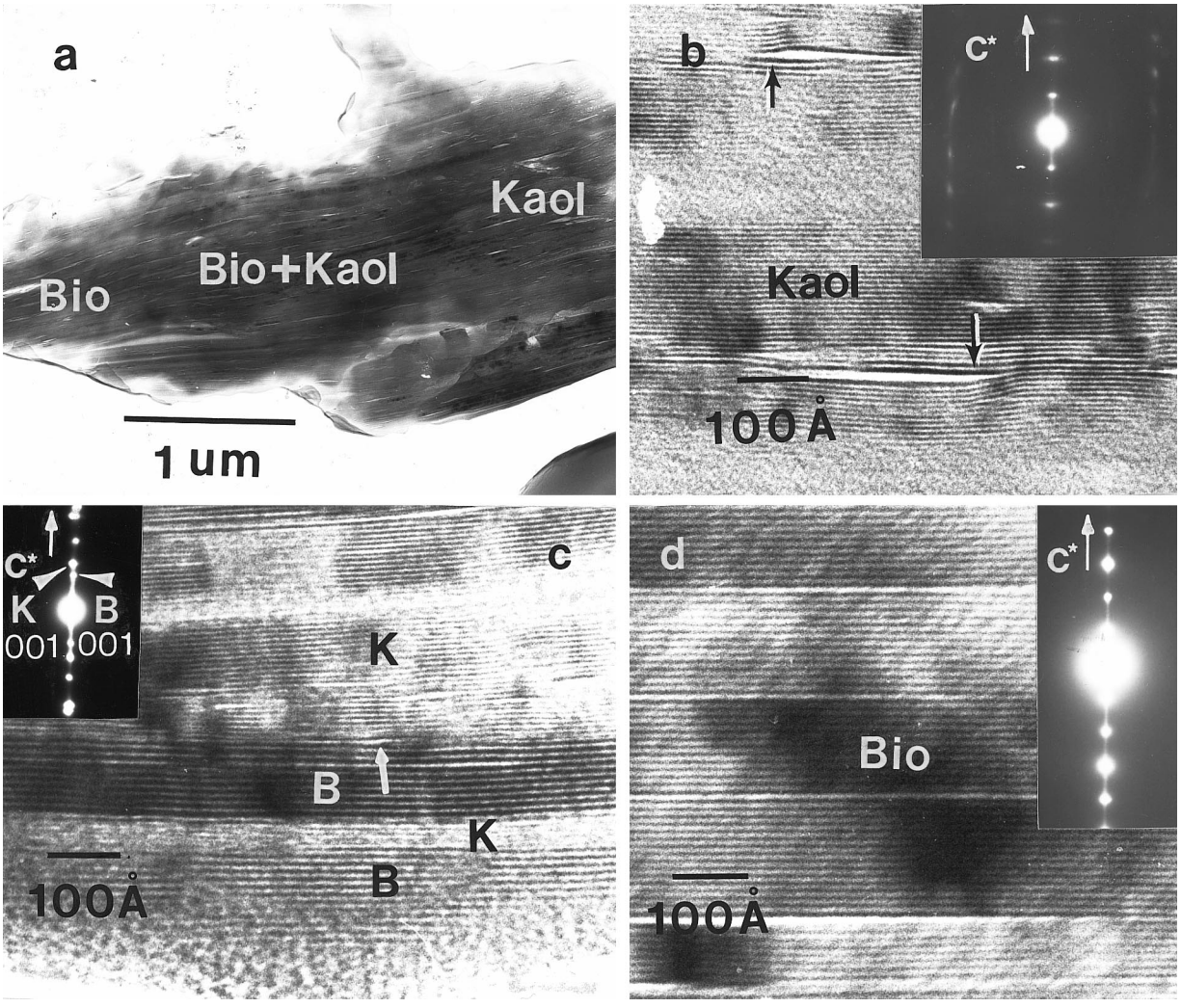


Fig. 6. TEM images of a phyllosilicate grain from saprolite at a depth of 714 cm. (a) Grain containing biotite and kaolinite layers. (b) Enlarged view of area in (a) marked Kaol. Most layers are 7 Å thick. Arrows point to lenses of an unidentified 7-Å phyllosilicate material. (c) Enlarged view of area in (a) marked Bio + Kaol. Note increase in thickness of kaolinite packet and corresponding decrease in thickness of biotite packet toward the right of the image. Arrow points to a junction of a single 10.5-Å layer diverging into two 8.5-Å layers, which thin to 7-Å layers. (d) Enlarged view of area in (a) marked Bio. Most layers are 10.5 Å thick; some 14-Å layers are also present.

layers (Fig. 6c, see arrow). STEM-EDS analyses showed that these layers contained approximately equal amounts of Al and Si with some Fe (Dong et al., 1998). This composition, along with the 8.5-Å layer spacing, suggests this phase is halloysite, which may have a layer spacing varying from 7 to 10 Å depending on the degree of hydration (Dixon, 1989).

If the mechanism of transformation is dissolution followed by precipitation (as suggested by Ahn and Peacor, 1987), then access of water into the interior of the phyllosilicate grains is necessary. Such access could be facilitated by the many cracks and pores visible at the edges of the phyllosilicate grains (Fig. 3). The high surface area of the biotite ($\sim$8 $m^2\ g^{-1}$) and the low average density of the phyllosilicate grains ($\sim$2.5 g $cm^{-3}$) as compared to the densities of biotite (2.7–3.3 g $cm^{-3}$), chlorite (2.6–3.3 g $cm^{-3}$), and kaolinite (2.6–2.8 g $cm^{-3}$; Deer et al., 1992), presumably reflects this high internal porosity.

### 5.2. Stoichiometry of Biotite Weathering

In order to quantify the rate of biotite weathering for comparison to laboratory measurements, the reaction mechanism must be identified. Three mechanisms are considered below.

Swoboda-Colberg and Drever (1993) assumed that biotite dissolved stoichiometrically with no secondary precipitation, because the system was far undersaturated with respect to secondary minerals. A possible reaction (assuming a pH of $\sim$4.6) of congruent dissolution of biotite would be

$$\begin{aligned} K_{0.65}(Al_{1.10}Ti_{0.15}Fe^{2+}_{0.35}Fe^{3+}_{0.15}Mg_{0.55})(Si_{3.2}Al_{0.8})O_{10}(OH)_2 \\ + 1.1H_2O + 8.6H_2CO_3 \Rightarrow 3.2H_4SiO_4 + 1.9Al^{3+} \\ + 0.65K^+ + 0.55Mg^{2+} + 0.35Fe^{2+} + 0.15Fe^{3+} \\ + 0.15TiO_2 + 8.6HCO_3^- \end{aligned} \quad (3)$$

The biotite composition used here is that determined by STEM-EDS for saprolite biotite (Table 2) (biotite and kaolinite were too intimately mixed to determine a composition of the saprolite biotite with electron microprobe). This equation predicts a Si/Mg release ratio of 5.8, which differs significantly from the observed ratio in the porewaters of the Luquillo saprolite ($\approx$ 3.5; White et al., 1998).

Alternatively, lattice fringe imaging under TEM suggests the transformation of one layer of biotite to two layers of kaolinite:

$$K_{0.65}(Al_{1.10}Ti_{0.15}Fe^{2+}_{0.35}Fe^{3+}_{0.15}Mg_{0.55})(Si_{3.2}Al_{0.8})O_{10}(OH)_2 + 0.8H_4SiO_4 + 2.1Al^{3+} + 3.4HCO_3^- + 3.1H_2O \Rightarrow 2Al_2Si_2O_5(OH)_4 + 0.65K^+ + 0.55Mg^{2+} + 0.35Fe^{2+} + 0.15Fe^{3+} + 0.15TiO_2 + 3.4H_2CO_3 \quad (4)$$

The reaction produces stoichiometric kaolinite and assumes that the discrepancy from stoichiometry of our STEM compositional analyses for this phase (Table 2) is related to incorporated impurity phases rather than incorporation of components into the kaolinite lattice. This reaction stoichiometry predicts that silica uptake occurs and, therefore, cannot explain the observed Si increase with depth in porewaters.

Finally, because Al is nearly conservative in the bulk regolith (White et al., 1998), we can write the stoichiometry assuming aluminum dissolved from biotite is conserved as kaolinite:

$$K_{0.65}(Al_{1.10}Ti_{0.15}Fe^{2+}_{0.35}Fe^{3+}_{0.15}Mg_{0.55})(Si_{3.2}Al_{0.8})O_{10}(OH)_2 + 2.05\ H_2O + 2.9\ H_2CO_3 \Rightarrow 0.95\ Al_2Si_2O_5(OH)_4 + 0.65K^+ + 0.55Mg^{2+} + 0.35Fe^{2+} + 0.15Fe^{3+} + 0.15TiO_2 + 1.3H_4SiO_4 + 2.9HCO_3^- \quad (5)$$

The predicted ratio of release rates of Si/Mg from this stoichiometry is 2.4, lower than the observed release rate (3.5), but closer than the predicted ratios based upon stoichiometries expressed by Eqns. 3 and 4.

If several mechanisms of biotite dissolution were occurring in the profile (for example, direct dissolution by Eqn. 3 and also biotite to kaolinite transformation by Eqns. 4 and/or 5), then an average Si/Mg ratio of 3.5 could be generated. However, sustaining biotite dissolution via Eqn. 3 would require significant aqueous transport of Al, and this is inconsistent with the low observed Al concentrations in the deeper porewater (White et al., 1998) and the low Al inorganic solubility. Alternatively, the higher observed release rate ratio of Si/Mg (3.5) in the regolith could be caused by dissolution of quartz or kaolinite throughout the profile. However, because the volume fraction of kaolinite increases upward in the profile, kaolinite is probably precipitating, rather than dissolving. Kaolinite precipitation is also supported by thermodynamic supersaturation of porewaters (White et al., 1998). The observation of etch pits on quartz grains is consistent with quartz dissolution (White et al., 1998).

### 5.3. Quantification of the Biotite Weathering Rate

There are no significant amounts of Mg- and K-bearing minerals other than biotite in the regolith; therefore, biotite weathering is the only reaction adding Mg and K to the soil solutions within the regolith profile. Magnesium precipitation is also negligible. Furthermore, the effect of ion exchange at this site is expected to be low, due to the lack of vermiculite or smectite and the limited sorption capacity of kaolinite. Therefore, the rate of Mg release from weathering of the phyllosilicate grains normalized to land surface area, $R_{phyllo}$ ($mol_{Mg}$ $m_{soil}^{-2}$ $s^{-1}$), is the normalized difference between the flux of Mg at any depth (z) and that entering the regolith at the surface, and can be expressed as

$$R_{phyllo} = q_z C_z - q_0 C_0 \quad (6)$$

where $q$ is average water flux (L $m_{soil}^{-2}$ $s^{-1}$), and $C$ is concentration ($mol_{Mg}$ $L^{-1}$) at any depth in the regolith (subscript $z$) or at the top of the regolith profile (subscript 0) (see Table 3 for glossary of symbols). The term $q_z$ is estimated to be $3.4 \times 10^{-5}$ L $m_{soil}^{-2}$ $s^{-1}$ based on the flux density in the upper saprolite at estimated field head gradient and moisture saturation (White et al., 1998). This value lies between the watershed infiltration rate estimated for base flow in the Rio Icacos ($2.23 \times 10^{-5}$ L $m_{soil}^{-2}$ $s^{-1}$, Santiago-Riviera, 1992) and that estimated for average flow ($1.17 \times 10^{-4}$ L $m_{soil}^{-2}$ $s^{-1}$, McDowell and Asbury, 1994).

Average Mg concentrations (cf. Table 4, White et al., 1998) at the saprolite/bedrock interface and in throughfall are 59.3 $\mu$M and 13.2 $\mu$M, respectively. Therefore, a simple calculation considering Mg concentrations and flux suggests a land-area normalized biotite dissolution rate in the regolith of 500 mol Mg $hectare^{-1}$ $yr^{-1}$ ($1.6 \times 10^{-9}$ $mol_{Mg}$ $m_{soil}^{-2}$ $s^{-1}$). This rate is comparable to the weathering rate estimated at the scale of the Rio Icacos watershed, ~1100 mol Mg $hectare^{-1}$ $yr^{-1}$ ($3.5 \times 10^{-9}$ $mol_{Mg}$ $m_{soil}^{-2}$ $s^{-1}$) (White and Blum, 1995). These values suggest that approximately one-half the biotite dissolution flux occurs in the regolith and one-half occurs deeper in the system.

If the soil and saprolite were homogeneous and porous, and there was no interflow, the total flux of water through a unit area of soil or saprolite at the top of the regolith ($q_0$) should equal the flux of water at any depth ($q_z$). Also, the flux of Mg

Table 3. Glossary of symbols

| | |
|---|---|
| $R_{phyllo}(z)$ | rate of release of Mg from phyllosilicate grain at depth z, normalized to phyllosilicate grain surface area ($mol_{Mg}$ $m_{phyllo}^{-2}$ $s^{-1}$) |
| $R_{biotite}(z)$ | rate of release Mg from biotite at depth z, normalized to biotite surface area ($mol_{Mg}$ $m_{biotite}^{-2}$ $s^{-1}$) |
| $z$ | depth in the regolith profile ($m_{soil}$) |
| $z_0$ | shallowest depth in regolith at which porewater chemistry is not affected by evapotranspiration ($m_{soil}$) |
| $C_z^{Mg}$ | concentration of Mg in porewater at depth $z$ ($mol_{Mg}$ $L^{-1}$) |
| $C_0^{Mg}$ | concentration of Mg in porewater at depth $z_0$ ($mol_{Mg}$ $L^{-1}$) |
| $q_0$ | flux of water at top of regolith (L $m_{soil}^{-2}$ $s^{-1}$) |
| $q_z$ | flux of water at depth $z$ (L $m_{soil}^{-2}$ $s^{-1}$) |
| $\alpha$ | area of phyllosilicate per area soil ($m_{phyllo}^2$ $m_{soil}^{-2}$) |
| $V_{phyllo}(z)$ | volume of phyllosilicate grains/volume of soil grains at depth $z$ ($m_{phyllo}^3$ $m_{\Sigma\ all\ minerals}^{-3}$) |
| $\rho_{phyllo}$ | density of phyllosilicate grain ($g_{phyllo}$ $m_{phyllo}^{-3}$) |
| $S_{phyllo}$ | surface area of phyllosilicate grain ($m_{phyllo}^2$ $g_{phyllo}^{-1}$) |
| $n(z)$ | porosity of soil at depth $z$ ($m_{void}^3$ $m_{soil}^{-3}$) |
| $X_{biotite}(z)$ | proportion of biotite in phyllosilicate grains at depth $z$ ($m_{biotite}^3$ $m_{phyllo}^{-3}$) |

through a unit area of soil or saprolite at the top of the regolith ($q_0\ C_0^{Mg}$) should equal the sum of the flux of Mg at any depth ($q_z C_z^{Mg}$) plus the rate of dissolution of phyllosilicate, $R_{phyllo}$, multiplied by a field mineral surface area term, $\alpha$:

$$q_0 C_0^{Mg} = q_z C_z^{Mg} + R_{phyllo}\alpha \quad (7)$$

Here, $R_{phyllo}$ is the rate normalized by the BET surface area of the phyllosilicate. The term $\alpha$ is related to the volume fraction of phyllosilicate grains in the regolith ($V_{phyllo}$), density of the phyllosilicate grains ($\rho_{phyllo}$), surface area of phyllosilicate grains ($S_{phyllo}$), porosity of the regolith as a function of depth ($n(z)$), and the depth ($z$):

$$\alpha = V_{phyllophyllo} S_{phyllo}\ (1 - n(z))\ z \quad (8)$$

White et al. (1998) have shown that the upper 120 cm of the regolith is heavily affected by evapotranspiration and interflow; therefore, we assume that $z_0$ must be set equal to a depth of at least 120 cm, below which we can assume little effect from these phenomena. The change in concentration with depth is written as the differential, *dC/dz*. The average water flux at any depth in the saprolite is assumed to be constant, so $q_0$ is equal to $q_z$. The equation thus becomes

$$R_{phyllo} = \left(\frac{dC}{dz}\right)\left(\frac{q_z}{V_{phyllo}(z)\rho_{phyllo}(1 - n(z))S_{phyllo}}\right) \quad (9)$$

where *dC/dz* is defined for depths $\geq$ 120 cm. The rate of change of concentration of Mg as a function of depth ($dC/dz = 8.0\ \mu$M Mg $m^{-1}$) was derived from a linear regression of solute chemistry vs. depth summarized in Table 5 of White et al. (1998). For this calculation, we also assume $\rho_{phyllo}$ and $S_{phyllo}$ are constants, equal to the measured values of 2.5 g $cm^{-3}$ and 8.2 $m^2\ g^{-1}$, respectively.

Equation 9 yields the rate of release of Mg from the phyllosilicate grains, normalized by surface area of phyllosilicate. To normalize the release rate by biotite surface area requires measurement of $S_{bio}$ rather than $S_{phyllo}$. We assume that the surface area can be partitioned between biotite and kaolinite by multiplication of $S_{phyllo}$ by the volume fraction of biotite in phyllosilicate grains, $X_{bio}(z)$. The assumption that surface area can be partitioned by the volume fraction of minerals is a standard, though untested, practice in quantification of mineral rates (e.g., White, 1995). The estimation of $X_{bio}(z)$ was discussed earlier and revealed that the fraction of biotite in the grains varies from <15% to approximately 30% of the total volume (Fig. 4c). This normalization does not take into account the fact that the biotite is armored by kaolinite, which decreases the amount of surface area of biotite directly exposed to weathering.

#### 5.3.1. Rate of magnesium release

Eqn. 9 can now be used to recalculate the release rate of Mg normalized by biotite surface area, $R_{bio}$, as a function of depth:

$$R_{bio} = \left(\frac{dC}{dz}\right)\left(\frac{q_z}{V_{phyllo}(z)\rho_{phyllo}(1 - n(z))S_{phyllo}X_{biotite}(z)}\right) \quad (10)$$

This equation gives a mean release rate of $6 \times 10^{-16}$ $mol_{Mg}$ $m_{biotite}^{-2}$ $s^{-1}$ (Fig. 7a). Calculating this release rate as the rate of biotite dissolution, according to Eqn. 5 (assuming the release of Mg from the octahedral sheet represents the rate of biotite dissolution and assuming a formula unit of $O_{10}(OH)_2$), yields $11 \times 10^{-16}$ $mol_{biotite}$ $m_{biotite}^{-2}$ $s^{-1}$.

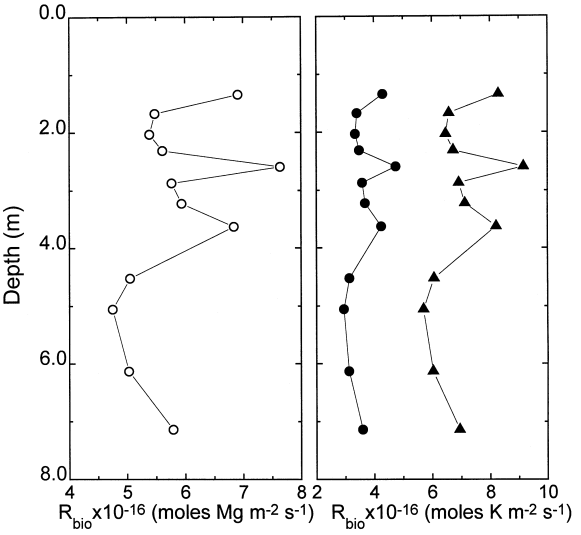


Fig. 7. (a) Release rate of Mg from biotite, normalized by biotite surface area (BET). (b) Release rate of K from biotite, normalized by biotite surface area (BET) (circles), and the release rate of K from biotite calculated from reaction *5*, using the Mg release rate from Fig. 7a (triangles).

#### 5.3.2. Rate of potassium release

The mean rate of K release calculated from Eqn. 10 by insertion of K concentration as a function of depth is $4 \times 10^{-16}$ $mol_K$ $m_{biotite}^{-2}$ $s^{-1}$ (Fig. 7b). The trend of K release from biotite with depth is similar to that of Mg release. The actual release rate of K is smaller than the rate of $7 \times 10^{-16}$ $mol_K$ $m_{biotite}^{-2}$ $s^{-1}$ that would be predicted from the Mg release rate if stoichiometric biotite dissolution was assumed to occur (Fig. 7b). If the release rate of K controlled biotite dissolution, this would give a biotite dissolution rate (as calculated from Eqn. 5) of $6 \times 10^{-16}$ $mol_{biotite}$ $m_{biotite}^{-2}$ $s^{-1}$. Less-than-stoichiometric K release from mica in short-term experiments was observed by Lin and Clemency (1981) and Acker and Bricker (1992), who attributed the lower K flux to the lack of K ions near the edges of the grains after initial leaching. In our samples, it is possible that an initial K release may have occurred in the bedrock or in the bedrock/saprolite transition zone, perhaps accompanying oxidation of Fe in the biotite.

### 5.4. Comparison of Release Rates to Laboratory Studies

The value of Mg release obtained from this study is 3–4 orders of magnitude slower than the rates obtained by laboratory studies (Table 1). Of the previously summarized factors thought to contribute to such a discrepancy in other systems, in this case, four factors seem important: (1) difference in mechanism between laboratory and field dissolution, (2) difference in solution chemistry between laboratory and field, (3) the presence of a mineral coating (kaolinite) occluding the reactive

biotite surface area in the regolith, and (4) heterogeneities of flow path. These possibilities are discussed below.

This case study represents an example in which the laboratory experiments probably measured dissolution rates occurring by dissimilar mechanisms from that of the field system. It is probable that in most of the laboratory studies, an interlayered vermiculite-biotite alteration product formed. Thus the mechanism of dissolution in the tropical system (biotite to kaolinite) was dissimilar to the mechanism in the laboratory (biotite to hydrobiotite). Only rates measured for the same mechanism of dissolution can be extrapolated safely.

Laboratory dissolution experiments tend to be run under far-from-equilibrium conditions (e.g., Swoboda-Colberg and Drever, 1993), in contrast to the solutions found in the Luquillo soils (White et al., 1998). High concentrations of K, Si, Mg, and Al may inhibit dissolution of biotite in these saprolites, either through an affinity effect, inhibition by an adsorbed species, or by the lowered diffusion gradients in the Nernst boundary layers at the mineral surface as observed for other silicates (White and Brantley, 1995). However, electrolyte effects on the dissolution kinetics of biotite at low temperature have been observed to be much smaller than the discrepancy described in this study (Kalinowski and Schweda, 1996). It is also possible that the higher concentration of solutes causes the difference in alteration mechanism which was observed.

In this study, the reactive surface contributing to weathering is most likely much lower than that measured by BET (see for example, Turpault and Trotignon, 1994). For example, element mapping revealed that the altered biotite is often surrounded by kaolinite. Therefore, little of the biotite may be in contact with solution, and cations released from the biotite would have to diffuse through the surrounding kaolinite. To account for this, a model would need to quantify the shrinking core of biotite, and the rate of diffusion across the boundary layer or kaolinite layer. Although the surface area of the phyllosilicate grains measured by BET was extremely high, corresponding to the many pores and cracks observed with SEM, these pores and cracks may have been dominated by kaolinite, rather than biotite surfaces. Furthermore, as pointed out by Kalinowski and Schweda (1996), the total BET surface area may not be the appropriate normalizing factor for mica dissolution occurring by an edge mechanism. For mica dissolution, extrapolating from the laboratory to the field may be particularly intractable unless models incorporating the geometry of dissolution (edge vs. layer) are developed.

Finally, as in every laboratory-field extrapolation, heterogeneities in fluid flow in the field system may further exacerbate the difficulty in extrapolating surface area-normalized rates of mineral dissolution (Swoboda-Colberg and Drever, 1993; Velbel, 1993). Where flow occurs along macropores in saprolite, dissolution may be minimized due to a lack of surface area intercepted. Flow through the matrix (micropores), on the other hand, should intercept significant biotite surface area, but dissolution may be slower overall due to higher solute concentrations (White and Brantley, 1995). Furthermore, flow may not be consistently vertical throughout the saprolite.

Our calculated biotite dissolution rate is also 1–3 orders of magnitude lower than rates estimated for other field systems (Table 1). Some of this discrepancy can be explained by our use of a BET surface area rather than a geometric surface area to normalize our rates. Mechanisms of dissolution of biotite may also differ among the three field studies summarized in Table 1.

## 6. CONCLUSION

Two different biotite weathering schemes occur in a saprolite/bedrock profile in the Rio Icacos watershed in Puerto Rico. Biotite in the bedrock has been partially altered to chlorite prior to disaggregation and formation of saprolite, but chlorite is almost entirely absent in the saprolite. Chlorite is presumed to weather rapidly to kaolinite in the cohesive zone between saprolite and bedrock, which was not sampled. Some of this early-formed kaolinite may remain in the macroscopic phyllosilicate grains found in the regolith and may persist throughout the saprolite profile from the bedrock/saprolite interface to a depth of 50 cm from the soil/air interface. However, because the biotite/kaolinite ratio increases with increasing depth in the saprolite below 120 cm (both in bulk saprolite and in individual phyllosilicate grains), a second mode of alteration must also occur in which the biotite in the saprolite weathers to kaolinite. TEM, SEM, and porewater chemistry provide evidence for such a transformation. TEM lattice fringe images reveal that two layers of kaolinite in the phyllosilicate grains commonly terminate at a single layer of biotite. The biotite-to-kaolinite transformation appears to occur at discrete boundaries, involving biotite dissolution and epitaxial kaolinite precipitation. This kaolinitization generally occurs from the edges of the phyllosilicate grain and moves inward, leaving a shrinking core of biotite within the phyllosilicate grain. This study provides the first documented microstructural (TEM) evidence for the biotite-kaolinite transformation in a weathering environment.

The rate of release of Mg from biotite in the profile, calculated as a flux through the regolith normalized per watershed land area, 500 mol hectare$^{-1}$ yr$^{-1}$ ($1.6 \times 10^{-9}$ $mol_{Mg}$ $m_{soil}^{-2}$ $s^{-1}$), is approximately one-half the flux estimated from Mg discharge out the Rio Icacos (1100 mol hectare$^{-1}$ yr$^{-1}$, or $3.5 \times 10^{-9}$ $mol_{Mg}$ $m_{soil}^{-2}$ $s^{-1}$), indicating that scaling up from the regolith to the watershed is consistent with a model whereby approximately half of the Mg released from the watershed is dissolved from biotite in the regolith, while the other half is dissolved from bedrock deeper in the system.

The rate of release of Mg from biotite in the profile, when normalized by BET surface area of biotite, is on the order of $10^{-16}$ $mol_{Mg}$ $m_{biotite}^{-2}$ $s^{-1}$, which is 3 orders of magnitude slower than the rate of Mg release observed in laboratory studies. The large discrepancy indicates that scaling down from the regolith to the lab reactor is not successful for this system. Potassium release is estimated at similar levels, but is slightly less than stoichiometric. The Si/Mg ratio of the release rates in the regolith porewaters do not match any simple biotite dissolution stoichiometries. This observation suggests either that several mechanisms are operative in the regolith or that quartz dissolution is occurring. Quartz dissolution is consistent with the porewater stoichiometries and the observed etching of quartz grains.

Little is known about the mechanism of biotite dissolution in the laboratory dissolution experiments which have been previously published (Table 1). However, it is safe to assume that the mechanism of dissolution in the laboratory is different from that observed in the field, obviating against accurate extrapo-

lation of laboratory rates to this tropical system. In addition, the high concentration of dissolved components in the soil porewater probably contributes to the slow release of cations from the biotite as compared to laboratory experiments. Furthermore, because biotite dissolves and reprecipitates as kaolinite on the biotite grains, the BET method of surface area determination used in this study probably overestimates the reactive surface area. The biotite in the regolith is surrounded at least partially by a rim of kaolinite; we infer that cations must pass through or around this kaolinite barrier to be released to porewaters. Normalization of mica dissolution rates by total rather than edge surface area is generally problematic wherever edge mechanisms dominate dissolution. Finally, as in virtually all laboratory to field extrapolations of mineral dissolution, our lack of data concerning coupled heterogeneities in fluid flow and chemistry makes it impossible to predict dissolution accurately from laboratory rates.

*Acknowledgments*—The Department of Geosciences at Penn State University and Shepherd Miller, Inc. provided support and assistance. Funding was provided by Grant #EAR-94-06263 from the National Science Foundation. Personnel associated with the Water, Energy, and Biogeochemical Budgets program of the United States Geological Survey provided invaluable assistance in this project: M. Larsen, R. Stallard, M. Schulz, and A. Torres participated in several aspects of field work and analysis. The STEM used in this study was acquired under Grant #EAR-87-08276 to D. Peacor of the University of Michigan from the National Science Foundation. D. Voigt, D. Peacor, A. Rose, B. Turner, P. Richards, and G. Kacandes provided helpful discussions and advice. Comments by T. Paces, P. Schweda, and an anonymous reviewer helped to improve the manuscript.

*Editorial handling:* T. Paces

## REFERENCES

Acker J. G. and Bricker O. P. (1992) The influence of pH on biotite dissolution and alteration kinetics at low temperature. *Geochim. Cosmochim. Acta* **56,** 3073–3092.

Ahn J. H. and Peacor D. R. (1987) Kaolinitization of biotite: TEM data and implications for an alteration mechanism. *Amer. Mineral.* **72,** 353–356.

American Geological Institute (1976) *Dictionary of Geological Terms.* Anchor Press.

Anbeek C. (1993) The effect of natural weathering on dissolution rates. *Geochim. Cosmochim. Acta* **57,** 4963–4975.

Banfield J. F. and Eggleton R. A. (1988) Transmission Electron Microscope study of biotite weathering. *Clays Clay Mineral.* **36,** 47–60.

Boccheciamp R. A. (1977) *Soil Survey of the Humacao Area of Eastern Puerto Rico.* USDA Soil Conserv. Serv.

Borchardt G. A. (1989) Smectites. In *Minerals in Soil Environments* (ed. J. B. Dixon and S. B. Weed), pp. 675–727. Soil Sci. Soc. Amer.

Brantley S. L. (1992) Kinetics of dissolution and precipitation-experimental and field results. *Proc. 7th Int. Symp. Water-Rock Interaction* 3–6.

Brantley S. L. and Chen Y. (1995) Chemical weathering rates of pyroxenes and amphiboles. In *Chemical Weathering Rates of Silicate Minerals* (ed. A. F. White and S. L. Brantley); *Mineral Soc. Amer. Short Course* **31** 119–172. MSA.

Brantley S. L., Crane S. R., Crerar D., Hellmann R., and Stallard R. (1986) Dissolution at dislocation etch pits in quartz. *Geochim. Cosmochim. Acta* **50,** 2349–2361.

Brown S., Lugo A. E., Silander S., and Liegel L. (1983) Research history and opportunities in Luquillo Experimental Forest, USDA Forest Serv. Gen. Tech. Rept. SO-44.

Deer W. A., Howie R. A., and Zussman J. (1992) *An Introduction to the Rock Forming Minerals.* 2nd ed. Longman Group Ltd.

Dixon J. B. (1989) Kaolin and serpentine group minerals. In *Minerals in Soil Environments* (ed. J. B. Dixon and S. B. Weed), pp. 467–525, Soil Sci. Soc. Amer.

Dong H., Peacor D. R., and Murphy S. F. (1998) TEM study of progressive alteration of igneous biotite to kaolinite throughout a weathered soil profile. *Geochim. Cosmochim. Acta* (in press).

Douglas L. A. (1989) Vermiculites. In *Minerals in Soil Environments* (ed. J. B. Dixon and S. B. Weed), pp. 635–727. Soil Sci. Soc. Amer.

Eswaran H. and Heng Y. Y. (1976) The weathering of biotite in a profile on gneiss in Malaysia. *Geoderma* **16,** 9–20.

Fanning D. S., Keramidas V. Z., and El-Desoky M. A. (1989) Micas. In *Minerals in Soil Environments* (ed. J. B. Dixon and S. B. Weed), pp. 551–634. Soil Sci. Soc. Amer.

Fordham A. W. (1990) Treatment of microanalyses of intimately mixed products of mica weathering. *Clays Clay Mineral.* **38,** 179–186.

Gilkes R. J. and Suddhiprakarn A. (1979) Biotite alteration in deeply weathered granite. II. The oriented growth of secondary minerals. *Clays Clay Mineral.* **27,** 361–367.

Goldich S. S. (1938) A study in rock weathering. *J. Geol.* **46,** 17–48.

Goldich S. S. (1984) Determination of ferrous iron in silicate rocks. *Chem. Geol.* **42,** 343–347.

Hutchison C. S. (1974) *Laboratory Handbook of Petrographic Techniques.* Wiley.

Jiang W., Peacor D. R., Merriman R. J., and Roberts B. (1990) Transmission and analytical electron microscopic study of mixed-layer illite/smectite formed as an apparent replacement product of diagenetic illite. *Clays Clay Mineral.* **38,** 449–468.

Kalinowski B. E. and Schweda P. (1996) Kinetics of muscovite, phlogopite, and biotite dissolution and alteration at pH 1–4, room temperature. *Geochim. Cosmochim. Acta* **60,** 367–387.

Kalpage F. S. C. P. (1974) *Tropical Soils.* The Macmillan Company of India Limited.

Lin F. and Clemency C. V. (1981) Dissolution kinetics of phlogopite. I. Closed-system. *Clays Clay Mineral.* **29,** 101–106.

Lowell S. and Shields J. E. (1991) *Powder Surface Area and Porosity.* Chapman and Hall.

Malla P. B. and Douglas L. A. (1987) Identification of expanding layer silicates: Charge density vs. expansion properties. *Proc. Int. Clay Conf.* (ed. H. van Olphen et al.) pp. 277–283. Clay Minerals Soc.

May H. M., Acker J. G., Smyth J. R., Bricker O. P., and Dyar M. D. (1995) Aqueous dissolution of low-iron chlorite in dilute acid solutions at 25°C. *Clay Minerals Soc.* **23,** 88 (abstr.).

McDowell W. H. and Asbury C. E. (1994) Export of carbon, nitrogen, and major ions from three tropical montane watersheds. *Limnol. Oceanogr.* **39,** 111–125.

Mehra O. P. and Jackson M. L. (1960) Iron oxide removal from soils and clays by a dithionite-citrate system buffered with sodium carbonate. *Proc. 7th Natl. Conf. Clays Clay Mineral.*, 317–327.

Meybeck M. (1979) Concentrations des eaux fluviales en éléments apports en solution aux océans. *Rev. Géogr. Dynam. Géol. Phys.* **21,** 215–246.

Milliman J. D. and Meade R. H. (1983) World-wide delivery of river sediment to the oceans. *J. Geol.* **91,** 1–21.

Moore D. M. and Reynolds R. C. (1989) *X-ray Diffraction and Identification and Analysis of Clay Minerals.* Oxford Press.

Murphy S. F. (1995) The weathering of biotite in a tropical forest soil, Luquillo Mountains, Puerto Rico. Master's thesis, Penn. State Univ.

Nagy K. L. (1995) Dissolution and precipitation kinetics of sheet silicates. In *Chemical Weathering Rates of Silicate Minerals,* (ed. A. F. White and S. L. Brantley); *Mineral. Soc. Amer. Short Course* **31,** 173–234. MSA.

Ojanuga A. G. (1973) Weathering of biotite in soils of a humid tropical climate. *Soil Sci. Soc. Amer. Proc.* **37,** 644–646.

Rausell-Colom J. A., Sweatman T. R., Wells C. B., and Norrish K. (1965) Studies in the artificial weathering of mica. In *Experimental Pedology* (ed. E. G. Hallsworth and D. V. Crawford), pp. 40–72. Butterworths.

Rebertus R. A., Weed S. B., and Buol S. W. (1986) Transformations of biotite to kaolinite during saprolite-soil weathering. *Soil Sci. Soc. Amer. J.* **50,** 810–819.

Reynolds R. C. (1985) NEWMOD© a computer program for the calculation of one-dimensional diffraction patterns of mixed-layered clays. R. C. Reynolds.

Santiago-Rivera L. (1992) Low-flow characteristics at selected sites on streams in Eastern Puerto Rico. U.S. Geological Survey WRI 92-4063.

Sawhney B. L. (1989) Interstratification in layer silicates. In *Minerals in Soil Environments* (ed. J. B. Dixon and S. B. Weed), pp. 789–828. Soil Sci. Soc. Amer.

Sawhney B. L. and Voigt G. K. (1969) Chemical and biological weathering in vermiculite from Transvaal. *Soil Sci. Soc. Amer. Proc.* **33,** 625–629.

Schnitzer M. and Kodama H. (1976) The dissolution of micas by fulvic acid. *Geoderma* **15,** 381–391.

Seiders V. M. (1971) Cretaceous and Lower Tertiary Stratigraphy of the Gurabo and El Yunque Quadrangles, Puerto Rico. USGS Bull. 1294-F.

Speer J. A. (1984) Micas in Igneous Rocks. In *Micas* (ed. S. W. Bailey); *Rev. Mineral.* **13,** 299–356. MSA.

Stoch L. and Sikora W. (1976) Transformation of micas in the process of kaolinization of granites and gneisses. *Clays Clay Mineral.* **24,** 156–162.

Sverdrup H. U. (1990) *The Kinetics of Base Cation Release due to Chemical Weathering.* Lund Univ. Press.

Swoboda-Colberg N. G. and Drever J. I. (1993) Mineral dissolution rates in plot-scale field and laboratory experiments. *Chem. Geol.* **105,** 51–69.

Tan K. H. (1980) The release of silicon, aluminum, and potassium during decomposition of soil minerals by humic acid. *Soil Sci.* **129,** 5–11.

Turpault M. P. and Trotignon L. (1994) The dissolution of biotite single crystals in dilute $HNO_3$ at 24°C: Evidence of an anisotropic corrosion process of micas in acidic solutions. *Geochim. Cosmochim. Acta* **58,** 2761–2775.

Van Grinsven J. J. M. and van Riemsdijk W. H. (1992) Evaluation of batch and column techniques to measure weathering rates in soils. *Geoderma* **52,** 41–57.

Velbel M. A. (1985) Geochemical mass balances and weathering rates in forested watersheds of the southern blue ridge. *Amer. J. Sci.* **285,** 904–930.

Velbel M. A. (1993) Constancy of silicate-mineral weathering-rate ratios between natural and experimental weathering: Implications for hydrologic control of differences in absolute rates. *Chem. Geol.* **105,** 89–99.

White A. F. (1995) Chemical weathering rates of silicate minerals in soils. In *Chemical Weathering Rates of Silicate Minerals* (ed. A. F. White and S. L. Brantley); *Mineral. Soc. Amer. Short Course* Vol. **31,** 407–461. MSA.

White A. F. and Blum A. E. (1995) Effects of climate on chemical weathering rates in watersheds. *Geochim. Cosmochim. Acta* **59,** 1729–1747.

White A. F. and Brantley S. L. (1995) Chemical weathering rates of silicate minerals: An overview. In *Chemical Weathering Rates of Silicate Minerals* (ed. A. F. White and S. L. Brantley); *Mineral. Soc. Amer. Short Course* **31,** 1–22. MSA.

White A. F. et al. (1997) Chemical weathering in a tropical watershed, Luquillo Mountains, Puerto Rico. I. Long-term versus short-term weathering fluxes. *Geochim. Cosmochim. Acta* **62,** 211–228 (this issue).

Whittig L. D. and Allardice W. R. (1986) X-ray diffraction techniques. In *Methods of Soil Analysis, Part 1: Physical and Mineralogical Methods* (ed. A. Klute), pp. 331–362. Soil Sci. Soc. Amer.

Wood W. W., Kraemer T. F., and Hearn P. P., Jr. (1990) Intragranular diffusion: An important mechanism influencing solute transport in clastic aquifers? *Science* **247,** 1569–1572.